九州大学大学院総合理工学府報告
第 44 巻 第 2 号 20-31 頁 令和 5 年 2 月

Engineering Sciences Reports, Kyushu University
Vol. 44, No. 2, pp. 20-31, FEB, 2023

Thermodynamic properties of Cu–Pb–F ternary system for the development of fluoride-ion batteries

Shangping ZHU[*1] Hideyuki HARADA[*2] Shoya KAWANO[*2]
Kumiko YAMAMOTO[*2] Hidenori MIKI[*3] Takeshi TOJIGAMORI[*3]
Kousuke NOI[*3] and Satoshi IIKUBO[*1, *2, †]
[†]E-mail of corresponding author: iikubo.satoshi.472@m.kyushu-u.ac.jp

(Received November 30, 2022, accepted December 7, 2022)

A thermodynamic analysis of the Cu-Pb-F ternary system was performed by incorporating first-principles calculations into the CALPHAD method. To evaluate the Gibbs energy, the phonon calculation was applied for some fluorides of the binary and ternary compounds. In addition, the FCC interstitial model was considered for the fluorides of Cu and Pb. For the Cu-Pb binary system, it is in good agreement with the experiment data. As for F-contained binary and ternary system, Gibbs energies of the stoichiometric compounds obtained by thermodynamic analysis are in good agreement with the phonon calculation, in which the existence of F makes it difficult to be investigated by experiment. Nevertheless, the data near $CuPb_2F_6$ shows significant discrepancy between phonon calculation data and experiment data, which may be the reason for the inaccurate reported $CuPb_2F_6$ crystal structure. Therefore, the crystal structure of reported $CuPb_2F_6$ was refined by neutron diffraction (ND) and atomic pair distribution function (PDF), in which the location of F atoms was obviously different after refinement. The formation energy of the refined structure based on CuF_2 and PbF_2 is -9.494 kJ/mol of atoms, whereas the unrefined structure is 3.550 kJ/mol of atoms, which shows the refined structure is more stable. The results of this study were helpful to clarify the phase equilibria of Cu-Pb-F system in the fluoride ion battery.

Key words: *phase diagram, first-principles calculations, CALPHAD, fluoride*

1. Introduction

Fluoride-ion batteries based on fluoride anions, which have the highest electronegativity, are promising candidates as alternatives to lithium-ion batteries.[1)] Relevant fluoride ion conductors have been studied in terms of their crystal structure, defects, ionic dynamics, etc.[2-3)] Among the reported fast fluoride-ion conductors, (1-x) PbF_2 ・ xMF_2(Mg, Ca, Sr, Ba) exhibits outstanding ionic conductivity of up to nearly 10^{-4} $S{\cdot}cm^{-1}$.[4-5)] Copper, which exhibits high electron conductivity, can also be treated as an alternative candidate for a doping material. In this field, knowledge regarding the phase stability of compounds in the Cu-Pb-F system is an important factor in fundamental studies, and basic information is often obtained from phase diagrams. Although it is difficult to collect systematic experimental data on phase equilibria, the calculation of phase diagrams (CALPHAD) method[6)] is a useful approach for calculating phase diagrams in multi-component and multi-phase systems.

The CuF_2–PbF_2 experimental pseudo binary phase diagram was obtained by M. Samouël.[7)] The X-ray diffraction pattern and crystal structure of $CuPb_2F_6$ were also reported by Samouel et al.[8)] Furthermore, Vaajamo et al. investigated the Cu–Pb binary phase diagram.[9)] However, the other ternary compound ($CuPbF_6$) reported by B. G. Müller et al.[10)] was not manifested in the reported phase diagram, and Cu–F and Pb–F binary phase diagrams have not been investigated thus far, which makes it difficult to collect experimental data. On the other hand, Johto et al.[11)] noted that the thermodynamic properties of the Cu–Pb–S ternary system

*1 Department of Advanced Energy Engineering Science
*2 Graduate School of Life Science and Systems Engineering, Kyushu Institute of Technology, Kitakyushu 808-0196, Japan
*3 Advanced Material Engineering Division, Higashifuji Technical Center, Toyota Motor Corporation, 1200 Mishuku, Susono, Shizuoka 410-1193, Japan.

were critically assessed and optimized using the CALPHAD method and showed good agreement with the experimental results.

To determine the difference between the calculated and experimental data, atomic pair distribution function (PDF) analysis of the neutron powder diffraction data has been used to compare the calculated PDF with the experimental PDF and refine the crystal structure parameters.[12-13] PDF structure modeling programs include small box modeling methods,[14] which use few parameters, and big box modeling programs,[15] which vary the number of atoms to maximize the agreement between the calculated and experimental PDFs. There are three widely used PDF structure modeling programs: PDFgui,[16] TOPAS,[17] and diffpy-cmi.[18]

In this study, first-principles calculations were used to perform thermodynamic assessments of stoichiometric compounds using the CALPHAD method. The Gibbs energy at finite temperatures was estimated by the finite displacement method;[19-20] then, the phase diagram was created using PANDAT software,[21] and the result was optimized based on experimental data. The difference between the realistic structure of $CuPb_2F_6$ and the reported structure was revealed, and refinement of the reported structure was carried out using neutron diffraction and the PDFgui program. The objective of this study was to clarify the phase equilibria of the Cu–Pb–F ternary system over the entire composition and phase stability of ternary compounds.

2. Experimental procedure

2.1. Synthesis of $CuPb_2F_6$ and X-ray diffraction (XRD)

Pure PbF_2 powder and pure CuF_2 powder with a ratio of 2:1 was synthesized using a planetary ball milling machine at room temperature. To ensure a single-phase solid solution was obtained, milling was performed for 72 h at 200 rpm.

X-ray diffraction (XRD) measurements were used to analyze the sample. The XRD measurements were carried out with CuK_{α_1}(1.5406 Å) radiation, and the XRD data were analyzed using the Rietveld method to match the reported crystal structure. [7-8]

2.2 First-principles calculations

First-principles calculations were performed based on density functional theory (DFT) using the Vienna *ab initio* simulation package (VASP) code.[22, 23] The interaction between the ion core and valence electrons was described using the projector-augmented wave method.[24,25] The exchange and correlation functions were given by the generalized gradient approximation, as proposed by Perdew et al.[26, 27] For structural optimization and enthalpy calculations, we set the plane wave energy cutoff to 520 eV. Brillouin zone sampling in a primitive cell was performed using a Γ-point-centered k-mesh that was limited to 0.15 $Å^{-1}$. The convergence criteria for electronic self-consistency and the ionic relaxation loop were set to 10^{-5} eV and 0.02 eV, respectively. The Methfessel–Paxton smearing method with a smearing width of 0.2 eV and the tetrahedron method with Blöchl corrections were used for structural optimization and the enthalpy calculation, respectively.

To examine the Helmholtz free energy, we conducted a first-principles phonon calculation based on the finite displacement method[19, 20] using the VASP code. The simplest approximation in lattice dynamics theory is a harmonic approximation. Once the phonon frequencies, ω, are solved under the harmonic approximation, the Helmholtz free energy, F, is calculated using the following equation:

$$F = \frac{1}{2}\sum_{qj} \hbar\omega_{qj} + k_B T \sum_{qj} \ln\left[1 - \exp\left(-\hbar\omega_{qj}/k_B T\right)\right], \quad (1)$$

where $\hbar$, k_B, T, q, and j are the reduced Planck constant, Boltzmann constant, temperature, wave vector, and phonon band index, respectively. For this phonon calculation, we used supercells to include an interaction range of approximately 10.0 Å with an atomic displacement distance of 0.02 Å. To estimate the force due to displacements within the DFT calculation, we used a plane wave energy cutoff of 400 eV, a convergence criterion for the electronic self-consistency loop of 10^{-6} eV, a Γ-point-centered k-mesh limited to 0.15 $Å^{-1}$, and the Methfessel–Paxton smearing method with a smearing width of 0.2 eV.

2.3 CALPHAD

2.3.1 FCC interstitial

The crystal structures of pure Cu and Pb are stable face-centered cubic (FCC) phases. Furthermore, the binary systems of Cu or Pb and F cannot be described by simply mixing the two elements where the Gibbs free energy of the system increases monotonically with the increase in F content, as this is inconsistent with reality. Therefore, we considered the FCC interstitial model for the fluorides of Cu and Pb. This model can describe invasion of the Cu or Pb FCC lattices by F atoms at vacancy sites. For instance, the Gibbs energy of the FCC interstitial phase is expressed using a two-sublattice model, in which the Pb atoms are substituted with Cu.

For example, the molar Gibbs energy of the FCC phase can be calculated using the following equation:

$$G^{FCC} = x_{\mathrm{Cu}}\,{}^{\circ}G^{FCC}_{\mathrm{Cu}} + x_{Pb}\,{}^{\circ}G^{FCC}_{Pb} + x_{\mathrm{F}}\,{}^{\circ}G^{FCC}_{\mathrm{F}} + RT(x_{\mathrm{Cu}}\,ln\,x_{\mathrm{Cu}} + x_{Pb}\,ln\,x_{Pb} + x_{\mathrm{F}}\,ln\,x_{\mathrm{F}}) + x_{\mathrm{Cu}}x_{Pb}L^{FCC}_{\mathrm{Cu,Pb}} + x_{Pb}x_{\mathrm{F}}L^{FCC}_{\mathrm{Pb,F}} + x_{\mathrm{Cu}}x_{\mathrm{F}}L^{FCC}_{\mathrm{Cu,F}} + x_{\mathrm{Cu}}x_{Pb}x_{\mathrm{F}}L^{FCC}_{\mathrm{Cu,Pb,F}} \quad (2)$$

where ${}^{\circ}G_i^{FCC}$ denotes the molar Gibbs energy of element i in the solid state, R is the universal gas constant, and the term x_i is the mole fraction of element i in the ternary system.

The lattice stability parameter is described by the following equation:

$${}^{\circ}G_i^{FCC} - {}^{\circ}H_i^{FCC} = a + bT + cT\,ln\,T + dT^2 + eT^3 + fT^7 + iT^{-1} + jT^{-9}, \quad (3)$$

where denotes the molar enthalpy of pure element i in its stable state at T = 25 ℃, and the symbols a–j are coefficients. This parameter denotes the interaction energy between i and j in the FCC phase, and it exhibits a compositional dependency following the Redlich–Kister polynomial:

$$L^{FCC}_{i,j} = {}^{0}L^{FCC}_{i,j} + {}^{1}L^{FCC}_{i,j}(x_i - x_j) + {}^{2}L^{FCC}_{i,j}(x_i - x_j)^2 + \cdots + {}^{n}L^{FCC}_{i,j}(x_i - x_j)^n, \quad (4)$$

where

$${}^{n}L^{FCC}_{i,j} = A + BT + CT\ln T + DT^2 + \cdots, \quad (5)$$

in which the symbols A–D are coefficients.

The FCC solid solutions, which exhibit a range of non-stoichiometric alloys, are modeled using the same FCC interstitial solution approximation.

2.3.2 Liquid phase

The molar Gibbs energy of the liquid phase, $G^{Liquid}_{A,B}$, is calculated using the following equation:

$$G^{Liquid}_{A,B} = x_A\,{}^{0}G^{Liquid}_{A} + x_B\,{}^{0}G^{Liquid}_{B} + RT\sum_{i=A}^{B} x_i \ln x_i + G^{Liquid}_{excess}, \quad (6)$$

where

$$G^{Liquid}_{excess} = x_A x_B[\,{}^{0}L^{Liquid}_{A,B} + {}^{1}L^{Liquid}_{A,B}(x_A - x_B) + {}^{2}L^{Liquid}_{A,B}(x_A - x_B)^2 \cdots], \quad (7)$$

in which G_i^{Liquid} denotes the molar Gibbs energy of element i in the liquid state, R is the universal gas constant, and x_i is the mole fraction of element i in the A–B binary system. G^{Liquid}_{excess} is the excess Gibbs energy in the system containing ${}^{n}L^{Liquid}_{A,B}$ that has a compositional dependency following the Redlich–Kister polynomial.

2.3.3 Gas phase

The gas phase of F was developed by Scientific Group Thermo data Europe (SGTE)[28] and provided by TCSAB.

2.3.4 Stoichiometric compounds

Binary compound phases with zero homogeneity ranges (i.e., CuF_2, PbF_2, PbF_3, and PbF_4) are treated as stoichiometric compounds. The Gibbs energies can be calculated using the phonon calculation and then fitted to equations.

2.3.5 Ternary compounds

In this study, two ternary phases were considered. The crystal structures of $CuPb_2F_6$ and $CuPbF_6$ were determined using the Pearson's crystal data. Then, the Gibbs energies of these phases were calculated using phonon calculation and curve fitting to equations to obtain their coefficients.

2.4 Neutron diffraction (ND) and data analysis

In this study, neutron diffraction (ND) was used to modify the reported crystal structure of $CuPb_2F_6$. Time-of-light (TOF) ND measurements were performed using the special-environment neutron diffractometer SPICA at the Japan Proton Accelerator Research Complex (J-PARC).[29] This instrument contains argon-filled position-sensitive detectors that are assembled in a

single detector–component box. The detector banks consist of a back-scattering bank and a multipurpose bank that are arranged from 175° to 5°, and the locations of these banks are approximately 2 m from the sample. The powder sample was placed in a cylindrical holder in which the atmosphere was completely replaced by argon gas, and the experiment was carried out at room temperature.

To visualize the crystal structure of the $CuPb_2F_6$ phase and create modified atom locations, full-profile fitting of the atomic PDF from the obtained ND data was performed using the PDFgui software. The experimental PDF was obtained from the Fourier transform of the structure factor. S(Q) is the neutron structure factor, which can be described by the following equation:

$$S(Q) = \frac{I(Q)}{Nb^2} = 1 + \int 4\pi r^2 \rho_0 [g(r) - 1] \frac{\sin(Qr)}{Qr} dr. \quad (8)$$

We can then obtain the experimental PDF, $G_{obs}(r)$, according to the Fourier transform, as follows:

$$G_{obs}(r) = \frac{2}{\pi} \int Q[S(Q) - 1] \sin(Qr)\, dQ. \quad (9)$$

When the crystal structure is previously known, the PDF can also be calculated using the PDFFIT program, and our equation for the model PDF becomes the following:[30]

$$G_{calc}(r) = \frac{1}{Nr} \sum_i \sum_{j \neq i} \left[\frac{b_i b_j}{\langle b \rangle^2} \delta(r - r_{ij}) \right] - 4\pi r \rho_0, \quad (10)$$

where $G_{calc}(r)$ is the model PDF for a single phase, ρ_0 is the average number density, N is the number of atoms, and $\langle b \rangle$ is the average scattering length; the indices i and j sum over all atom pairs in that phase, where b_i and b_j are the scattering lengths for atoms i and j, respectively, and r_{ij} is the separation distance between atoms i and j. Thus, the structural parameters of the calculation are refined to fit the experimental PDF to allow the crystal structure to be obtained. The calculation of the standard deviation is described by the R-value, and the expected R-value is defined as follows:

$$R_{exp} = \sqrt{\frac{N-p}{\sum_{i=1}^{N} w(r_i) G_{obs}^2(r_i)}}, \quad (11)$$

where G_{obs} is the experimental PDF, and the weight for each data point is given by $w(r_i)$. Therefore, the weighted R-value (R_w) is defined as follows:

$$R_w = \sqrt{\frac{\sum_{i=1}^{N} w(r_i)[G_{obs}(r_i) - G_{calc}(r_i)]^2}{\sum_{i=1}^{N} w(r_i) G_{obs}^2(r_i)}}. \quad (12)$$

Here, G_{calc} represents the calculation data. In this study, we obtained the PDF data for the experimental crystal structure using ND and PDFgui in the first step, and then the PDF data of the reported structure were also calculated using Equation (12). Therefore, the atoms of the reported structure could be moved to fit the experimental data, and thus the experimental crystal structure could be predicted based on the goodness-of-fit of the two data sets with low R_w.

3. Results and discussion

The space group and formation energy for the stoichiometric compounds of Cu-Pb-F system were list in Table A1, in which energy was calculated by First-principles calculation.

3.1 Cu–Pb binary system

The lattice stability parameters for the pure elements obtained from the SGTE databases[28] are listed in Table A2. The thermodynamic parameters for Cu–Pb are listed in Table 3, which are included in the Thermo-Calc SSOL4.9 database. The calculated Cu–Pb phase diagram is shown in Fig. 1 and is in good agreement with the experimental data.[31-33]

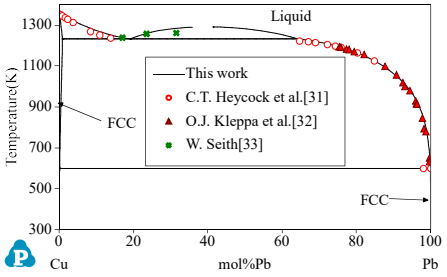

Fig.1 Calculated Cu–Pb phase diagram with experimental results.

3.2 Cu–F and Pb–F binary systems (FCC interstitial)

The Cu–F binary system consists of the liquid, gas, body-centered cubic (BCC), FCC, hexagonal close-packed (HCP), and CuF_2 phases The Pb–F binary system is composed of the liquid, gas, BCC, FCC, HCP, PbF_2_FCC, PbF_2_pnma, PbF_3, and PbF_4 phases. In this

study, the thermodynamic parameters were calculated using a first-principles calculation in which non-stoichiometric compounds used the FCC interstitial model. The database is listed in Table A3 and the calculated phase diagrams are shown in Fig. 2(a) and Fig. 3.

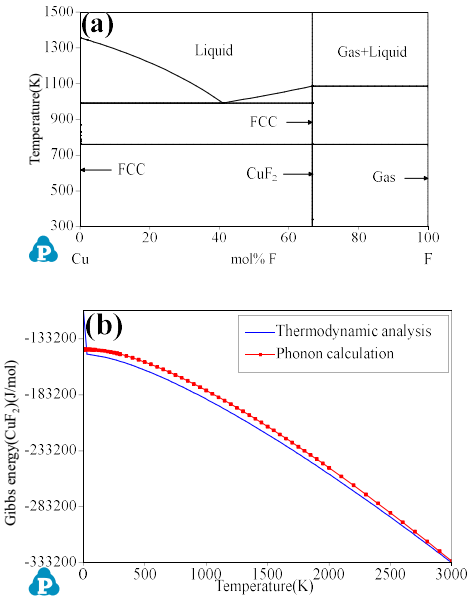

Fig.2 (a) Calculated Cu–F binary phase diagram, (b) Gibbs energy for CuF_2.

In the Cu–F binary phase diagram, the stoichiometric compound is CuF_2 with a melting point of 1109.15 K, which is the same as the experimental data. The eutectic point is located at 41% F and 992 K.

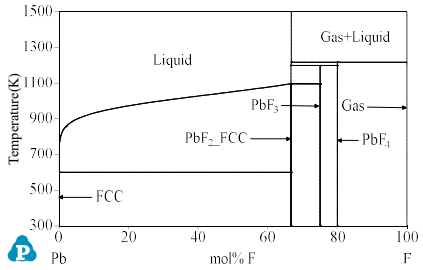

Fig.3 Calculated Pb–F binary phase diagram.

As shown in Fig. 2(a), F is stable as F_2, and thus the F_2 gas phase is displayed on the F-rich side. The CuF_2 phase is stable below 760 K, while the FCC interstitial (FCC-int) is stable above 760 K. We also matched the Gibbs energy of CuF_2 calculated by the thermodynamic and phonon calculation analyses described in Fig. 2(b), which shows that the results of the thermodynamic analysis are in good agreement with the results of the phonon calculation.

According to Fig. 3, the stoichiometric compounds consist of PbF_2_FCC, PbF_3, and PbF_4, in which PbF_2_FCC is always more stable than PbF_2_pnma. The FCC interstitial (FCC-int) in the Pb–F binary system is only stable below 600 K. Fig. 4 shows the Gibbs energy in the Pb–F system obtained by the phonon calculation and thermodynamic analysis. The results are in good agreement and indicate the stability of PbF_2_FCC.

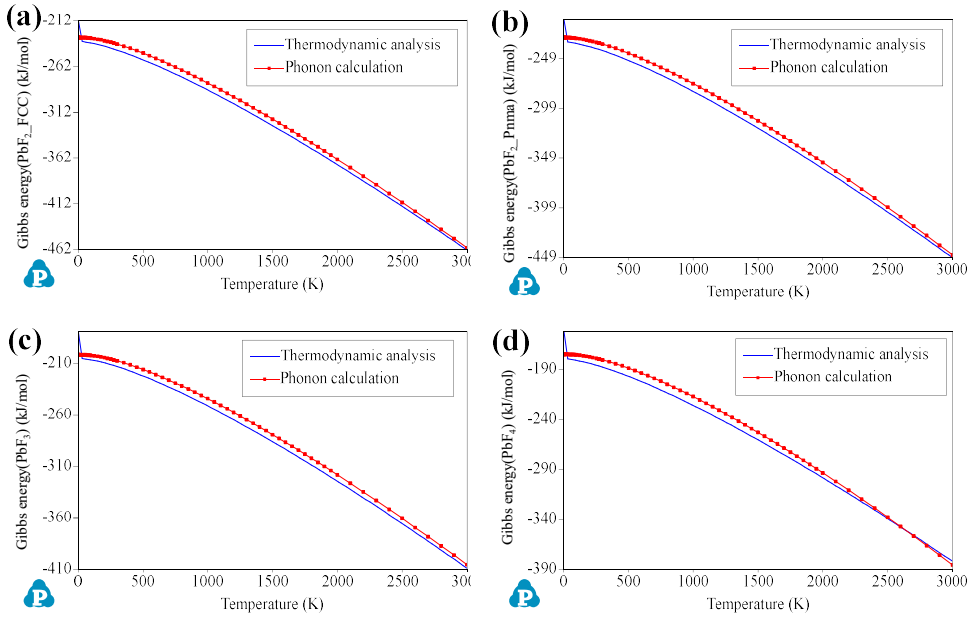

Fig.4 Gibbs energies of (a) PbF_2_FCC, (b) PbF_2_Pnma, (c) PbF_3, and (d) PbF_4.

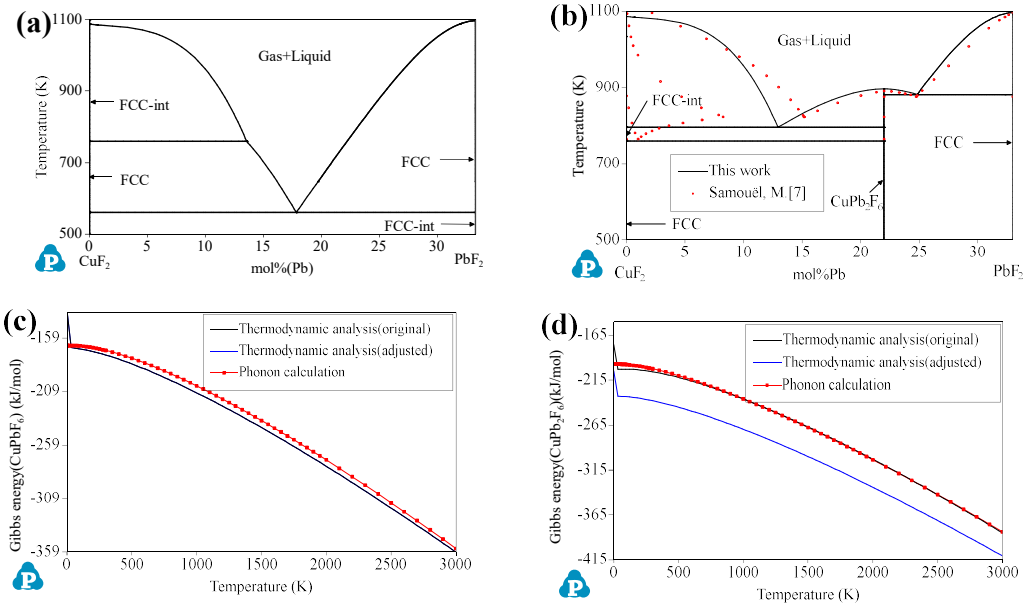

Fig.5 (a)original pseudo CuF_2-PbF_2 phase diagram (b)pseudo CuF_2-PbF_2 phase diagram adjusted by experimental data (c) Gibbs energy for $CuPbF_6$ in adjusted phase diagram(d) Gibbs energy for $CuPb_2F_6$ in original and adjusted phase diagram.

3.3 Cu–Pb–F ternary system

The Cu–Pb–F ternary phase diagram was calculated using the three binary systems above, and the ternary phases ($CuPbF_6$ and $CuPb_2F_6$) were calculated using phonon calculation and adjusted based on experimental data; the results are presented in Table A3 and Fig. 5. In Fig. 5(a) and (b), the Fig. 5(a) is the calculated pseudo-binary phase diagram of the CuF_2–PbF_2 system, in which the ternary phases just calculated by phonon calculation, and the Fig. 5(b) is adjusted by CuF_2–PbF_2 experimental data based on the Fig. 5(a). This result in Fig. 5(a), has big different with experimental data,[7] but the Fig. 5(b) is in good agreement with the experimental results obtained by M. Samouël.[7] In particular, the Pb-rich side is expected to cause the system to be in equilibrium. Otherwise, one of the ternary phases ($CuPb_2F_6$) appears on the pseudo phase diagram (Fig. 5(b)), which has been previously reported. In Fig. 5(c) and 5(d), the Gibbs energies of the $CuPbF_6$ and $CuPb_2F_6$ phases are shown, respectively, comparing the thermodynamic analysis data with the phonon calculation results. We note that the $CuPbF_6$ phase has no diversity within the two methods, but the Gibbs energy for the $CuPb_2F_6$ phase obtained from the phonon calculation is much higher than the thermodynamic analysis data which adjusted by experimental data. This shows a clear difference in $CuPb_2F_6$ before and after adjustment, which may be a result of the inaccuracy of the reported structure.

As shown in Fig. 6, the isothermal section of the Cu-Pb-F phase diagram was calculated at temperatures of 300 K, 500 K, 700 K, and 1000 K. At 300 K, it consists of all of the binary and ternary compounds reported, as shown in Fig. 6(a). In particular, the $CuPbF_6$ phase is present in the F-rich region, which did not appear in the experimental phase diagram. When temperature increases to 500 K, as shown in Fig. 6(b), the $CuPbF_6$ phase disappears and is disassembled into CuF_2 and PbF_4 phases, while the other phases remain. Thus, the stable temperature range of the $CuPbF_6$ phase is below 500 K. Furthermore, a small region of PbF_2_FCC+Liquid appears next to the Pb–F binary side at 700 K, as shown in Fig. 6(c), because the melting point of Pb is 600 K. The isothermal section at 1000 K is shown in Fig. 6(d). The CuF_2 phase is unstable and

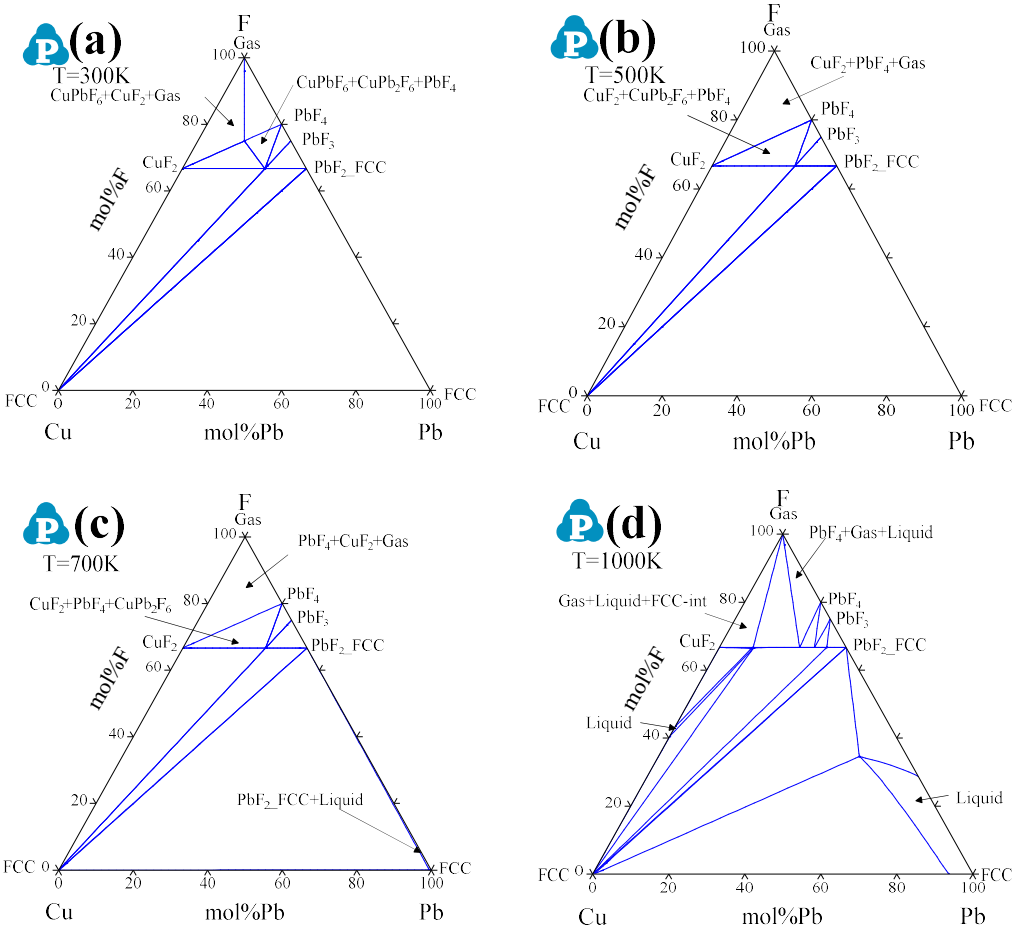

Fig.6 Isothermal sections of the Cu-Pb-F phase diagram: (a) 300 K, (b) 500 K, (c) 700 K, (d) 1000 K.

transforms into the FCC-int phase, and the $CuPb_2F_6$ is melted, as it has a melting point of 891 ℃. In contrast, the PbF_2_FCC, PbF_3, and PbF_4 phases remain stable. The liquid phase field extends continuously above the relevant eutectic points, in agreement with the binary phase diagrams described above.

3.4 XRD and ND

The crystal structure of $CuPb_2F_6$ was obtained from the experimental XRD data for the pure material synthesized using CuF_2 and PbF_2, as shown in Fig. 7(a) and 7(b). The phonon density of state (DOS) for $CuPb_2F_6$ was calculated using first-principles calculations, as shown in Fig. 7(c). The negative frequency of the phonon DOS accounts for 12.2% of the overall calculation, which indicates the dynamic instability of this crystal structure. Furthermore, the Gibbs energies of $CuPb_2F_6$ for the adjusted and unadjusted phase diagrams are inconsistent, which also indicates the inaccuracy of the crystal structure ascertained by XRD. The low sensitivity for light elements (e.g., Cu, F) in XRD may be the reason for the inaccurate $CuPb_2F_6$ structure.

Therefore, ND is employed to elucidate the structure owing to its high sensitivity, even for light elements. In Fig. 8(a), the experimental PDF is obtained using the Fourier transform of the reduced structure factor. We compared each peak of the experimental data with the F–F, Cu–Cu, Pb–Pb, Cu–F, Pb–F, and Cu–Pb pair calculation data to confirm the existence of atom pairs for each peak. The peaks are related to the F–F pair, except those near 3 and 6 Å, which were determined to be related to other pairs, particularly Cu–F and Pb–F. The peak at 20 Å is related to all atomic pairs, and thus the comparisons between the experiment and calculation are conducted from 0 to 19 Å. A comparison between the experimental data

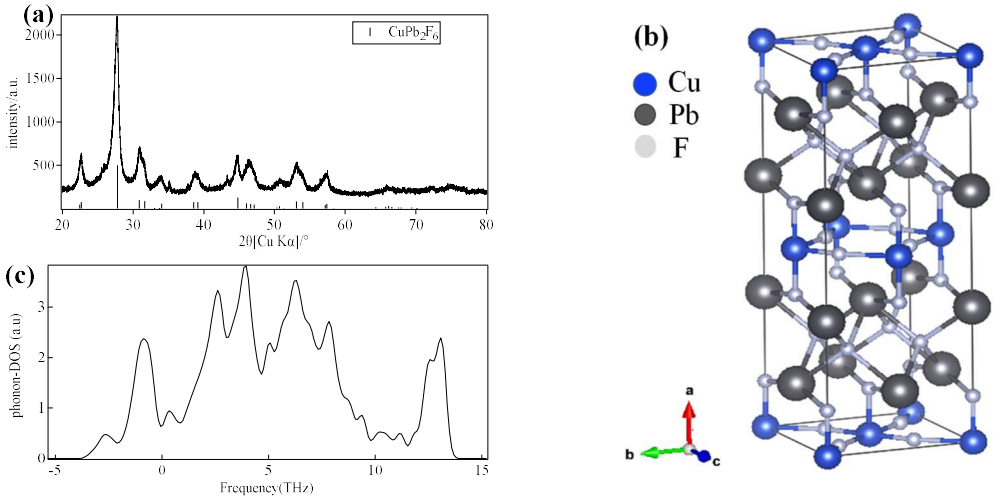

Fig.7 (a) XRD pattern for $CuPb_2F_6$, (b) reported crystal structure of $CuPb_2F_6$, (c) phonon density of state for the reported $CuPb_2F_6$ structure.

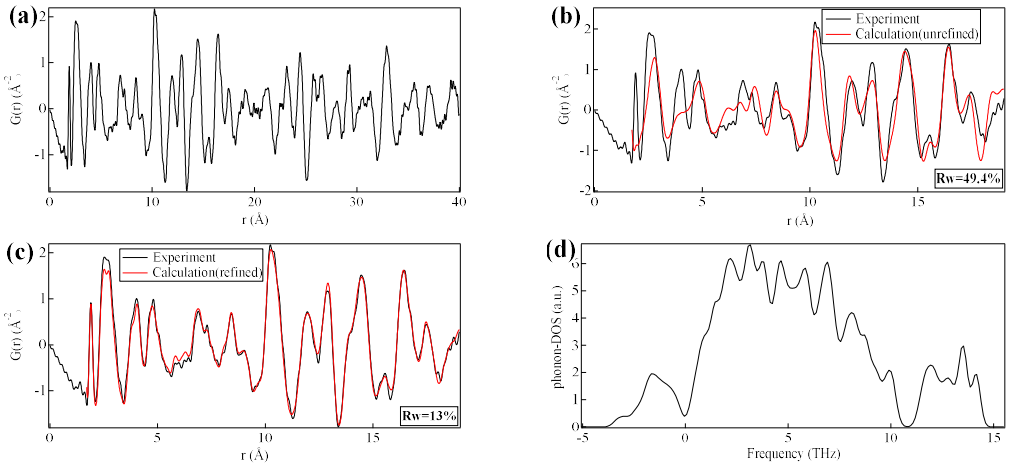

Fig.8 (a) Experimental neutron diffraction data transformed using PDFgui, (b) PDFs for the experiment and unrefined structure, (c) PDFs for the experiment and refined structure, (d) phonon calculation for the refined crystal structure of $CuPb_2F_6$.

and the calculation for the unrefined structure with a weighted R-value (R_w) of up to 49.4% is shown in Fig. 8(b). In Fig. 8(c), the standard deviation, R_w , between the experimental data and calculation data for the refined structure, which was refined by focusing on F–F, Cu–F, and Pb–F, decreases to 13%. The results in Fig. 8(a) and 8(b) show that the refined structure has good accuracy with a realistic structure. The phonon calculation for the refined structure shows that the negative frequency decreases to 6.8% compared to 12.2% for the unrefined structure, as shown in Fig. 8(d). There is still a small amount of negative frequency remaining, which may be because the first-principles phonon calculation with the finite displacement method was calculated at 0 K, and the ND was performed at room temperature.

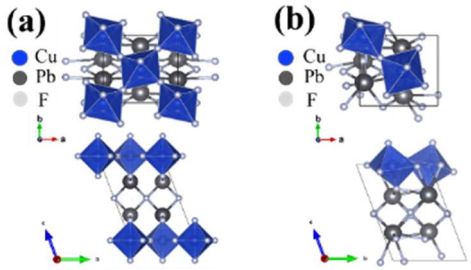

Fig.9 Structure of $CuPb_2F_6$: (a) unrefined, (b) refined.

The crystal structures of $CuPb_2F_6$ before and after refinement are shown in Fig. 9(a) and 9(b), respectively. In terms of the location of the atoms, there is no obvious difference for Cu and Pb, but the F atoms are obviously distorted. The structure of unrefined $CuPb_2F_6$ is an octahedron that rotates around the c-axis, whereas the refined structure rotates

around the a-axis and b-axis. The results show that the refined structure is locally distorted compared to the unrefined structure, and the formation energy based on CuF_2 and PbF_2 of the refined structure is -9.494 kJ/mol of atoms, which is more stable than CuF_2 and PbF_2, whereas the formation energy of the unrefined structure is 3.550 kJ/mol of atoms.

4. Conclusions

Thermodynamic analysis of the Cu–Pb–F system and atomic pair distribution function (PDF) analysis of neutron powder diffraction (ND) data were performed, yielding the following results.

(1) The Cu–F and Pb–F binary systems were calculated, and the Gibbs energies of the stoichiometric compounds calculated by thermodynamic analysis and phonon calculations were in good agreement. The FCC interstitial model was used to calculate the non-stoichiometric compounds, which FCC-int phase shows stable in the Isothermal sections of the Cu-Pb-F phase diagram at 1000 K. Although the reliability of the model still need to be validated, it is helpful to clarify the non-stoichiometric compounds.

(2) For the Cu–Pb–F ternary system, the calculated pseudo CuF_2–PbF_2 phase diagram showed good agreement with the experimental phase diagram, especially on the Pb-rich side, and the phase stability of all compounds was revealed in the isothermal section of the Cu–Pb–F phase diagram. Furthermore, a difference between the thermodynamic analysis and phonon calculation for $CuPb_2F_6$ was observed, which may be due to the accuracy of the reported $CuPb_2F_6$ structure.

(3) PDF and ND were performed to refine the crystal structure of $CuPb_2F_6$. The location of the F atoms was obviously different in the unrefined and refined structures, whereas the Cu and Pb atoms exhibited no obvious change, which is the reason why the reported structure obtained using XRD had low accuracy. Finally, the negative frequency remaining in the phonon calculation of the refined crystal structure may be caused by the fact that the phonon calculation was performed at 0 K and the ND was conducted at room temperature. It may be possible to use finite-temperature phonon calculations to obtain results with no negative frequency.

Acknowledgment

This paper is based on results obtained from a project, JPNP16001 and JPNP21006, commissioned by the New Energy and Industrial Technology Development Organization (NEDO).

References

1) A.A. Potanin, Solid-state secondary power supply,Google Patents, 2010.
2) K. Mori et al., Experimental Visualization of Interstitialcy Diffusion Pathways in Fast-Fluoride-Ion-Conducting Solid Electrolyte Ba0.6La0.4F2.4. ACS Applied Energy Materials 3, 2873-2880 (2020).
3) J. Chable et al., Fluoride solid electrolytes: investigation of the tysonite-type solid solutions La 1− x Ba x F 3− x (x< 0.15). Dalton Transactions 44, 19625-19635 (2015).
4) V. Tmovcoca et al., Fast ionic conductivity of Pb2 :MF2 (M=Mg, Ba, Cd) and PbF2 :ScF3 single crystals and composites. Solid State Ionics 119, 181-189(1999).
5) V. Y. Kavun et al., Ion mobility and transport in ß-PbF2 doped with alkaline-earth fluorides. Inorganic materials 43, 301-309 (2007).
6) N. Saunders, A. P. Miodownik, CALPHAD (calculation of phase diagrams): a comprehensive guide. (Elsevier, 1998).
7) M. Samouël, Equilibres de cristallisation dans onze sysemes de deux fluorures simples. Syntheses dans l'eta solide et identifications cristallographiques des fluorures doubles rencontres. Revwe de Chimie minerale 8, 537(1971).
8) M. Samouël, P. Gredin, A. de Kozak, Powder diffraction data for copper hexafluorides: Ba2CuF6 and Pb2CuF6. Powder Diffraction 10, 221-222 (1995).
9) I. Vaajamo, H. Johto, P. Taskinen, A thermodynamic assessment of the Cu-Fe-Pb ternary system. 4, 1283-1302 (2011).
10) B. G. Müller, F. Schrötter, Zur Kristallstruktur ternärer Cu(II)-Fluoride CuMIVF6 (MIV = Sn, Pb, Ti, Mn, Pd). 196, 261-268 (1991).
11) H. Johto, P. Taskinen, Phase stabilities and thermodynamic assessment of the system Cu–Pb–S. Minerals Engineering 42, 68-75 (2013).
12) H. Zhang, B. Gilbert, F. Huang, J. F. Banfield, Water-driven structure transformation in nanoparticles at room temperature. Nature 424, 1025-1029 (2003).
13) M. W. Terban et al., Early stage structural development of prototypical zeolitic imidazolate

framework (ZIF) in solution. Nanoscale 10, 4291-4300 (2018).
14) T. Egami, S. J. Billinge, Underneath the Bragg peaks: structural analysis of complex materials. (Newnes, 2012).
15) R. L. McGreevy, Reverse monte carlo modelling. Journal of Physics: Condensed Matter 13, R877 (2001).
16) C. Farrow et al., PDFfit2 and PDFgui: computer programs for studying nanostructure in crystals. Journal of Physics: Condensed Matter 19, 335219 (2007).
17) A. A. Coelho, TOPAS and TOPAS-Academic: an optimization program integrating computer algebra and crystallographic objects written in C++. Journal of Applied Crystallography 51, 210-218 (2018).
18) P. Juhás, C. L. Farrow, X. Yang, K. R. Knox, S. J. Billinge, Complex modeling: a strategy and software program for combining multiple information sources to solve ill posed structure and nanostructure inverse problems. Acta Crystallographica Section A 71, 562-568 (2015).
19) G. Kresse, J. Furthmüller, J. Hafner, Ab initio force constant approach to phonon dispersion relations of diamond and graphite. EPL (Europhysics Letters) 32, 729 (1995).
20) K. Parlinski, Z. Li, Y. Kawazoe, First-principles determination of the soft mode in cubic ZrO2. Physical Review Letters 78, 4063 (1997).
21) S.-L. Chen et al., The PANDAT software package and its applications. Calphad 26, 175-188 (2002).
22) G. Kresse, J. Furthmüller, Bayesian optimization for calibrating and selecting hybrid-density functional models. Phys. Rev. B 54, 11169-11186 (1996).
23) G. Kresse, J. Furthmuller, Comp Mater Sci. CAS Article 6 (1), 15–50 (1996).
24) P. E. Blöchl, Projector augmented-wave method. Physical Review B 50, 17953-17979 (1994).
25) G. Kresse, D. Joubert, From ultrasoft pseudopotentials to the projector augmented-wave method. Physical Review B 59, 1758-1775 (1999).
26) J. P. Perdew, K. Burke, M. Ernzerhof, Generalized Gradient Approximation Made Simple. Physical Review Letters 77, 3865-3868 (1996).
27) J. P. Perdew, K. Burke, M. Ernzerhof, Generalized Gradient Approximation Made Simple. Physical Review Letters 78, 1396-1396 (1997).
28) A. T. Dinsdale, SGTE data for pure elements. Calphad 15, 317-425 (1991).
29) M. Yonemura et al., Development of SPICA, New Dedicated Neutron Powder Diffractometer for Battery Studies. Journal of Physics: Conference Series 502, 012053 (2014).
30) T. Proffen, S. J. L. Billinge, PDFFIT, a program for full profile structural refinement of the atomic pair distribution function. Journal of Applied Crystallography 32, 572-575 (1999).
31) C. T. Heycock, F. H. Neville, Ii. complete freezing-point curves of binary alloys containing silver or copper together with another metal. Philosophical Transactions of the Royal Society of London. Series A, Containing Papers of a Mathematical or Physical Character, 25-69 (1897).
32) O.J. Kleppa and J.A. Wei, Solubility of Cu in liquid Pb below 950℃. Journal of the American Chemical Society 74, 6047-6051(1952).
33) W. Seith, H. Johnen, J. Wagner, Study of miscibility gap in the liquid in binary and ternary metallic systems, Z. Metallked 46, 773-779(1955).

Appendix

Table A1. Compounds of (Cu, Pb)F.

Formula	Space group	Formation Energy (kJ/mol of atom)
CuF_2	Fm-3m	-124.02
CuF_2	P2_1/c	-146.78
CuF	F-43m	-78.61
PbF_2	Fm-3m	-232.54
PbF_2	Pnma	-230.31
PbF_3	P-4c2	-205.26
PbF_4	I4-mmm	-178.86
$CuPb_2F_6$	C12-m1	-200.41
$CuPbF_6$	P-1	-169.95

Table A2. Lattice stability parameters for Cu, Pb, and F.

Species	Phase		Lattice stability parameter, J/mol	Temperature, K
Cu	L	${}^{\circ}G_{Cu}^{L} - {}^{\circ}G_{Cu}^{FCC}$	$=12964.736-9.511904T-5.849\times10^{-21}T^{7}$	$298.15 < T < 1357.77$
			$= 13495.481 - 9.922344T - 3.642 \times 10^{29}T^{-9}$	$1357.77 < T < 3200$
	FCC	${}^{\circ}G_{Cu}^{FCC} - {}^{\circ}H_{Cu}^{FCC}$	$= -7770.458 + 130.485235T - 24.112392T\ln T - 0.00265684T^{2} + 1.29223 \times 10^{-7}T^{3} + 52478T^{-1}$	$298.15 < T < 1357.77$
			$= -13542.026 + 183.803828T - 31.38T\ln T + 3.64167 \times 10^{29}T^{-9}$	$1357.77 < T < 3200$
	BCC	${}^{\circ}G_{Cu}^{BCC} - {}^{\circ}G_{Cu}^{FCC}$	$= 4017 - 1.255 \times T$	$298.15 < T < 6000$
	HCP			
Pb	FCC	${}^{\circ}G_{Pb}^{FCC} - {}^{\circ}H_{Pb}^{FCC}$	$= -7650.085 + 101.715188T - 24.5242231T\ln T - 0.00365895T^{2} - 2.4395 \times 10^{-7}T^{3}$	$298.15 < T < 601$
			$= -10531.115 + 154.258155T - 32.4913959T\ln T + 0.00154613T^{2} + 8.05644 \times 10^{25}T^{-9}$	$601 < T < 1200$
			$= 4157.596 + 53.154045T - 18.9640637T\ln T + 0.002882943T^{2} + 9.8144 \times 10^{-8}T^{3} - 2696755T^{-1} + 8.05644 \times 10^{25}T^{-9}$	$1200 < T < 5000$
	L	${}^{\circ}G_{Pb}^{L} - {}^{\circ}G_{Pb}^{FCC}$	$= 4672.157 - 7.750257T - 6.0144 \times 10^{-19}T^{7}$	$298.15 < T < 601$
			$= 4853.112 - 8.066587T - 8.05644 \times 10^{25}T^{-9}$	$601 < T < 5000$
F	MOLE_GAS	GGASF2	$= -9757.53536 - 3.03641497T - 29.08493T\ln T - 0.007466065T^{2} + 1.16183617 \times 10^{-6}T^{3} + 72117.3T^{-1}$	$298.15 < T < 800$
			$= -10225.5134 + 17.0719031T - 32.43806T\ln T - 0.0028914815T^{2} + 2.13090167 \times 10^{-7}T^{3} - 31206.07T^{-1}$	$800 < T < 2500$
			$= -75010.7092 + 286.369351T - 66.19232T\ln T + 0.004699418T^{2} - 9.36513 \times 10^{-8}T^{3} + 22790040T^{-1}$	$2500 < T < 6800$
			$= 79866.236 - 46.25962T - 28.00029T\ln T + 4.8653845 \times 10^{-4}T^{2} - 6.238305 \times 10^{-9}T^{3} - 96222900T^{-1}$	$6800 < T < 10000$
		GHSER	$= 0.5 \times$ GGASF2	

Table A3. Thermodynamic parameters for the binary and ternary systems.

System	Phase and model	Thermodynamic parameters, J/mol of model	Temperature, K	Ref.
Cu-Pb	L	${}^{0}L^{L}_{Cu,Pb} = 31008 - 7.195T$		[30]
		${}^{1}L^{L}_{Cu,Pb} = 15345 - 10.826T$	$298.15 < T < 6000$	
		${}^{2}L^{L}_{Cu,Pb} = -6493 + 5.947T$		
		${}^{3}L^{L}_{Cu,Pb} = -18416 + 13.16T$		
	FCC-int	${}^{0}L^{FCC}_{Cu,Pb:Va} = 28000 + 12T$	$298.15 < T < 3000$	
		${}^{1}L^{FCC}_{Cu,Pb:Va} = 100000$		
	BCC	${}^{\circ}G^{BCC}_{Cu,Pb:Va} = 45684 + 5.151T$	$298.15 < T < 6000$	
		${}^{\circ}G^{HCP}_{Cu,Pb:Va} = 50000$		
Cu-F	L	${}^{\circ}G^{L}_{CuF_2} - {}^{\circ}G^{L}_{Cu} - 2\,{}^{\circ}G^{L}_{F} = -280000 - 30T$	$298.15 < T < 3000$	This work
		${}^{\circ}G^{L}_{F} - {}^{\circ}G^{HSER}_{F_2}$=-4246.8+50T	$298.15 < T < 6000$	
		${}^{0}L^{L}_{Cu,CuF_2} = 0$	$298.15 < T < 3000$	
		${}^{0}L^{L}_{CuF_2,F} = 0$	$298.15 < T < 3000$	
	FCC-int	${}^{0}L^{FCC}_{Cu,F:Va} = 240000 + 10T$	$298.15 < T < 3000$	
		${}^{1}L^{FCC}_{Cu,F:Va} = -35000 + 25T$		
	CuF_2	${}^{\circ}G^{CuF_2}_{Cu:F} - {}^{\circ}G^{FCC}_{Cu} - 2\,{}^{\circ}G^{HSER}_{F_2} = -429527.9934 + 135.55T - 0.1T\ln T$		
Pb-F	L	${}^{\circ}G^{L}_{PbF_2} - {}^{\circ}G^{L}_{Pb} - 2\,{}^{\circ}G^{L}_{F} = -540000 - 10.7T$	$298.15 < T < 3000$	This work
		${}^{\circ}G^{FCC}_{PbF_2} - {}^{\circ}G^{L}_{Pb} - 2\,{}^{\circ}G^{L}_{F} = -689907.6204 + 128T - 0.3T\ln T$	$298.15 < T < 3000$	
		${}^{0}L^{L}_{Pb,PbF_2} = 0$	$298.15 < T < 3000$	
		${}^{0}L^{L}_{PbF_2,F} = 0$	$298.15 < T < 3000$	
	FCC-int	${}^{0}L^{FCC}_{Pb,F:Va} = 488000 + 30T$	$298.15 < T < 3000$	
		${}^{1}L^{FCC}_{Pb,F:Va} = 55000 + 25T$		
	PbF_2	${}^{\circ}G^{PbF_2\_FCC}_{F:Pb} - {}^{\circ}G^{FCC}_{Pb} - 2\,{}^{\circ}G^{HSER}_{F_2} = -689907.6204 + 128T - 0.3T\ln T$	$298.15 < T < 3000$	
		${}^{\circ}G^{PbF_2\_Pnma}_{F:Pb} - {}^{\circ}G^{FCC}_{Pb} - 2\,{}^{\circ}G^{HSER}_{F_2} = -682907.6204 + 136.5T + 0.001T\ln T$		
	PbF_3	${}^{\circ}G^{PbF_3}_{F:Pb} - {}^{\circ}G^{FCC}_{Pb} - 3\,{}^{\circ}G^{HSER}_{F_2} = -804786.388 + 208T - 0.02T\ln T$	$298.15 < T < 3000$	
	PbF_4	${}^{\circ}G^{PbF_4}_{F:Pb} - {}^{\circ}G^{FCC}_{Pb} - 4\,{}^{\circ}G^{HSER}_{F_2} = -877665.1557 + 260T + 0.9T\ln T$	$298.15 < T < 3000$	
Cu-Pb-F	L	${}^{0}L^{L}_{CuF_2,PbF_2} = -250000 - 20T$	$298.15 < T < 3000$	This work
		${}^{1}L^{L}_{CuF_2,PbF_2} = 100T$	$298.15 < T < 3000$	
	FCC-int	${}^{0}L^{FCC}_{Cu,Pb:F} = 32000 + 10T$	$298.15 < T < 3000$	
		${}^{1}L^{FCC}_{Cu,Pb:F} = 0$	$298.15 < T < 3000$	
	$CuPbF_6$	${}^{\circ}G^{CuPbF_6}_{Cu:F:Pb} - {}^{\circ}G^{FCC}_{Cu} - {}^{\circ}G^{FCC}_{Pb} - 6\,{}^{\circ}G^{HSER}_{F_2} = -1312693.149 + 420T - 0.5T\ln T$	$298.15 < T < 3000$	
	$CuPb_2F_6$	${}^{\circ}G^{CuPb_2F_6}_{Cu:F:Pb} - {}^{\circ}G^{FCC}_{Cu} - 2\,{}^{\circ}G^{FCC}_{Pb} - 6\,{}^{\circ}G^{HSER}_{F_2} = -2060000 + 503.8T - 1T\ln T$	$298.15 < T < 3000$	